J Mater Sci (2018) 53:13600–13616

Mechanochemical Synthesis

Toward a better conversion in magnesiothermic SHS of zirconium diboride

Sergio Cordova[1] and Evgeny Shafirovich[1,*]

[1] *Department of Mechanical Engineering, The University of Texas at El Paso, 500 W. University Ave, El Paso, TX 79968, USA*

Received: 31 January 2018
Accepted: 15 May 2018
Published online: 22 May 2018

ABSTRACT

Zirconium diboride (ZrB_2) is a promising ultra-high-temperature ceramic material. Magnesiothermic self-propagating high-temperature synthesis (SHS) is an attractive method for its fabrication from relatively inexpensive oxides of zirconium and boron. However, prior studies on magnesiothermic, combustion-based methods for synthesis of ZrB_2 have revealed incomplete conversion. The present work aims to determine optimal conditions for magnesiothermic SHS of ZrB_2 from ZrO_2 and B_2O_3. The addition of MgO, NaCl, and excess Mg was investigated experimentally. Mechanical activation (short-time high-energy ball milling) was used to facilitate ignition of the powder mixtures. After combustion in an argon environment, the products were leached by diluted HCl to remove magnesium compounds and NaCl. The results show that NaCl is a better additive than MgO; it effectively improves milling and decreases the amount of zirconia in the products. Further, NaCl decreases the particle size of the products, which is beneficial for sintering. The addition of excess Mg also has a positive effect on the conversion because it compensates for the loss of Mg through vaporization during the SHS process. In the products obtained by combustion and leaching of the mixtures with 20% excess Mg and 10–30 wt% NaCl, the oxygen content was below 4 wt%. Nanoscale polycrystalline ZrB_2 particles were obtained using the mixture with 20% excess Mg and 30 wt% NaCl.

Introduction

Diboride of zirconium (ZrB_2) belongs to the class of ultra-high-temperature ceramics (UHTC). In its hexagonal P6/*mmm* AlB_2-type structure [1–3], B–B and B–Zr covalent bonds cause chemical stability and a high melting point (3246 °C) [4], while Zr–Zr metallic bond leads to high electrical and thermal conductivities [5]. ZrB_2 is resistant to oxidation, has relatively low density (6.1 g/cm^3), and exhibits a good high-temperature strength. The unique properties of ZrB_2 make it a promising material for ultra-high-temperature applications such as hypersonic vehicles [6, 7] and electrodes in magnetohydrodynamic (MHD) generators [8]. Unfortunately, the

Address correspondence to E-mail: eshafirovich2@utep.edu

https://doi.org/10.1007/s10853-018-2460-8

current methods for production of ZrB_2 are complex, energy-consuming, and expensive. Therefore, it is important to develop new, low-cost techniques for large-scale fabrication of ZrB_2-based materials.

Although zirconium diboride can be produced by direct synthesis from elements, high costs of zirconium and boron make this approach unsuitable for large-scale applications [9]. Commonly studied methods for synthesis of ZrB_2 are based on the reduction of oxides, salts, or acids. Zirconia (ZrO_2) is usually used as the source of zirconium [9]. Also, zircon ($ZrSiO_4$) has been proposed recently [10, 11]. As the boron source, boron oxide (B_2O_3) is commonly used [9]. Other compounds such as boric acid (H_3BO_3) [12, 13] and, more recently, borax ($Na_2B_4O_7$) [14] have also been utilized.

ZrB_2 has been synthesized via borothermic and boron carbide–carbon reduction of ZrO_2 [15, 16]. Since both routes are endothermic processes, the procedures involved heating in a high-temperature furnace. In the case of borothermic reduction, the mixture was also milled for 70 h preceding the high-temperature synthesis step. Pure ZrB_2, however, was obtained only in the boron carbide–carbon reduction route, and this required the addition of excess B_4C and C. A similar method is carbothermic reduction of ZrO_2 and B_2O_3, which is also conducted in a furnace with a preceding milling step [17].

The great amounts of energy consumed in the endothermic reduction processes shift the interest to combustion synthesis approaches, where the released heat of exothermic chemical reactions provides energy for a self-sustained process and only a small amount of energy is needed for the initiation of this process [18–21]. Among the various combustion synthesis methods, self-propagating high-temperature synthesis (SHS) has been utilized for the fabrication of numerous intermetallics and ceramics [19, 20, 22–25]. In SHS, the compacted mixture of initial powders is ignited at one end, and the combustion wave propagates over the mixture, leading to the formation of the desired product. Advantages of SHS include fast processing times, simple equipment, high purity of products, and tailored microstructure [20, 21].

SHS of ZrB_2 from elemental Zr and B has been conducted as long as decades ago [26] following the reaction described by:

$$Zr + 2B \rightarrow ZrB_2; \Delta H^o_{rxn} = -323\,kJ \quad (1)$$

(Standard enthalpies of all reactions in the present paper have been calculated based on [27]). More recently, the addition of NaCl to Zr and B has enabled the fabrication of nanoscale ZrB_2 powder by SHS [28]. However, as already mentioned, synthesis from elements is not suitable for commercial production; a more economical SHS route involves metallothermic reduction of oxides, acids, or salts. Many materials (e.g., BN, W, TiC, WC, B_4C, Si, and Mo) have been fabricated by SHS with metallothermic reduction of oxides or salts [29–34].

A metal can be used as a reducing agent if the Gibbs energy of its oxide is lower than those of the oxides that have to be reduced. Aluminum is one such metal, but it is hard to separate alumina (Al_2O_3), a product of aluminothermic reduction, from ZrB_2. As a result, ZrB_2–Al_2O_3 composites have been obtained by aluminothermic combustion processes [35–37], but Al cannot be used for synthesis of pure ZrB_2.

In contrast with alumina, magnesia (MgO) can be removed by leaching with a mild acid such as diluted hydrochloric acid (HCl). This makes magnesiothermic reduction more attractive than the aluminothermic route when the goal is to obtain diborides and not diboride-oxide composites. For this reason, magnesiothermic reduction has been studied extensively for synthesis of ZrB_2.

As shown in the next section, a major problem in the magnesiothermic reduction route for synthesis of ZrB_2 is incomplete conversion of oxides to borides. The objective of the present work was to investigate the effects of adding MgO, NaCl, and excess Mg on the magnesiothermic MASHS of ZrB_2 from ZrO_2 and B_2O_3 with the goal of obtaining powder with low oxygen content and small particle size, which is desired for sintering [38]. In the SHS experiments, mechanical activation preceded the combustion process to facilitate the ignition. Leaching by diluted HCl acid was used for removing both MgO and NaCl from the products. The combustion process was studied using video recording, thermocouple measurements, while the products were examined with X-ray diffraction analysis and scanning electron microscopy.

Background

Here, we provide a brief review of experiments on ZrB_2 synthesis with magnesiothermic reduction, which involved SHS and other combustion-based methods such as thermal explosion (also called volume combustion synthesis, VCS) and mechanically induced self-sustained reaction (MSR). In VCS, the entire sample is heated uniformly in a furnace, which leads to ignition [18]. This method is usually used when the system is low-exothermic and requires significant preheating. The combustion temperature in VCS is higher than that of the same mixture during SHS because of the external energy input from the furnace. In MSR, ignition is caused by the collisions of grinding balls during milling [39]. It is difficult to scale up MSR because of the pressure increase inside of the milling vial and safety concerns.

It should be noted that mixtures for magnesiothermic SHS of ZrB_2 have a low exothermicity as compared with the stoichiometric Zr/B mixture, which makes the ignition difficult. This problem can be overcome in the so-called mechanically activated self-propagating high-temperature synthesis (MASHS), where mechanical activation, i.e., a short-duration, high-energy ball milling precedes the combustion process [40–42].

Setoudeh and Welham [43] obtained ZrB_2 by mechanochemical reaction in $ZrO_2/B_2O_3/Mg$ powder mixture, placed in a ball mill, according to the equation:

$$ZrO_2 + B_2O_3 + 5Mg \rightarrow ZrB_2 + 5MgO;\ \Delta H^o_{rxn} = -959\ \text{kJ} \quad (2)$$

After 15 h of mechanical alloying at 165 rpm in an argon atmosphere, the mixture was heated to 1200 °C. XRD analysis was conducted after different milling times, after heating, and after acid leaching. This analysis has shown that with increasing the milling time from 2 to 15 h, the amounts of ZrB_2 and MgO gradually increased, but peaks of ZrO_2 still remained even after 15 h of milling and subsequent heating to 1200 °C.

Khanra et al. [12, 13] conducted magnesiothermic combustion synthesis of ZrB_2. Although the authors identified the used method as SHS, in both studies, the mixtures were globally heated inside a furnace until ignition occurred, which classifies the used method as VCS (or thermal explosion). Boric acid was used as the boron source, and the desired chemical reaction is described by:

$$ZrO_2 + 2H_3BO_3 + 5Mg \rightarrow ZrB_2 + 5MgO + 3H_2O(g);\ \Delta H^o_{rxn} = -769\ \text{kJ} \quad (3)$$

ZrB_2 crystallite size, estimated using the Scherrer formula, decreased from 25 nm at 0 wt% NaCl to 13 nm at 20 wt% NaCl [12]. In [13], the authors focused on decreasing ZrO_2 impurities in the combustion products. For this purpose, pre-calculated amounts of Mg and H_3BO_3 were added to the leached products and a second VCS process was conducted inside the furnace. XRD analysis has shown that the second VCS step slightly increases the conversion of oxides to borides. However, it adds complexity and increases the processing time.

Mishra et al. investigated the magnesiothermic SHS of ZrB_2, using B_2O_3 as the source of boron [17] and following the stoichiometry (Eq. 2). Although impurities were not reported by the authors, unlabeled peaks in the presented XRD pattern apparently belong to ZrO_2. Nishiyama et al. [44] conducted magnesiothermic VCS of ZrB_2, using B_2O_3 as the precursor. Similarly to [12, 13], the obtained products consisted of ZrB_2 with ZrO_2 impurities.

Magnesiothermic synthesis of ZrB_2 according to Eq. (2) was also investigated by Akgün et al. [14]. They tested two methods—VCS and mechanical alloying. They have shown that VCS in air becomes possible if mechanical activation precedes heating. In both methods, they attempted to improve the conversion by increasing the concentrations of Mg and B_2O_3. However, even at 30% excess Mg and B_2O_3 residual ZrO_2 was detected in XRD patterns of the products.

Recently, the magnesiothermic MSR of ZrB_2 from ZrO_2 and B_2O_3 (Eq. 2) was studied by Jalaly et al. [45]. Ignition occurred after about 6 min of continuous milling with steel balls at 600 rpm in a 5-bar Ar atmosphere. After ignition, the mixture was mechanically alloyed for 3 h at the same rotation speed. XRD analysis was conducted before the MRS process, after ignition, after the mechanical alloying step, and after leaching in a 1 M HCl solution. After ignition, the dominant phases were ZrB_2 and MgO, but small peaks of Mg and ZrO_2 were also observed. Mechanical alloying for 3 h removed the peaks of Mg and ZrO_2, but the subsequent leaching led to the appearance of a small peak of ZrO_2.

The same authors also studied magnesiothermic MSR of ZrB_2/SiC/ZrC mixtures [10, 11], where the desired reaction is described by:

$$ZrSiO_4 + B_2O_3 + C + 7Mg \rightarrow ZrB_2 + SiC + 7MgO;\ \Delta H^o_{rxn} = -1235\ kJ \quad (4)$$

Ignition took place inside the bowl after 6-min milling, leading to the fabrication of ZrB_2, MgO, SiC, and ZrC phases with a small amount of zircon remained unreacted. Subsequent milling for 3 h removed the peaks of zircon. It was shown that Mg was the only reducing agent, while carbon acted only as a carbide-forming agent.

Zhang et al. synthesized ZrB_2 via molten-salt magnesiothermic reduction of ZrO_2 and borax [46] in a furnace. The desired reaction is described by:

$$2ZrO_2 + Na_2B_4O_7 + 10Mg \rightarrow 2ZrB_2 + 10MgO + Na_2O;\ \Delta H^o_{rxn} = -1604\ kJ \quad (5)$$

The mixtures that contained up to 30% excess Mg and $Na_2B_4O_7$ were heated at 800–1200 °C for 3 h in an argon environment. Impurities of ZrO_2 and $Mg_3B_2O_6$ were found in the experiments conducted at stoichiometry. Full conversion was reported for mixtures with 20% excess Mg and 30% excess $Na_2B_4O_7$, heated to 1200 °C. The authors, however, did not discuss the exothermicity of the involved reactions. To address this issue, we have conducted thermodynamic calculations of the adiabatic flame temperatures of those mixtures using THERMO (version 4.3) software, which is based on the Gibbs free energy minimization and contains a database of approximately 3000 compounds [47]. The calculations at an initial temperature of 25 °C at 1 atm pressure show that the adiabatic flame temperature is 2049 K (1776 °C) for the stoichiometry and 1937 K (1664 °C) for 20% excess Mg and 30% excess $Na_2B_4O_7$. This indicates that the actual temperature of the mixture during synthesis in the furnace was much higher than 1200 °C, which makes interpretation of their results difficult.

To clarify the reaction mechanisms during magnesiothermic SHS of ZrB_2, several authors have used differential scanning calorimetry (DSC) and thermogravimetric analysis (TGA). Khanra tested ZrO_2/H_3BO_3/Mg mixture with DSC and TGA in an argon flow [48]. It was reported that H_3BO_3 lost H_2O at 169 °C, so at higher temperatures the boron source in their mixture was actually B_2O_3. An exothermic peak was observed at 794 °C on the DSC curve.

Zheng et al. conducted DSC and TGA of milled ZrO_2/B_2O_3/Mg mixture in an argon flow [49]. The DSC curve revealed a large exothermic peak at 745 °C, i.e., at a bit lower temperature than in [48].

Jalaly et al. [45] performed DSC of an unmilled ZrO_2/B_2O_3/Mg mixture. In these tests, in addition to an exothermic peak at 850 °C, there was an exothermic peak at 640 °C, just before the endothermic peak of Mg melting. Based on the XRD analysis of samples quenched at 600, 750, and 1000 °C, the authors concluded that the first exothermic peak was caused by the reaction of Mg with B_2O_3:

$$B_2O_3 + 3Mg \rightarrow 2B + 3MgO;\ \Delta H^o_{rxn} = -532\ kJ \quad (6)$$

while the second exothermic peak was caused by the reaction of Mg with ZrO_2:

$$ZrO_2 + 2Mg \rightarrow Zr + 2MgO;\ \Delta H^o_{rxn} = -105\ kJ \quad (7)$$

Apparently, the formed Zr immediately reacts with already available B according to Eq. (1), so the two steps form a single exothermic peak on the DSC curve. XRD analysis of samples quenched at 1200 and 1400 °C has shown gradual improvement of the oxide-to-boride conversion with increasing the temperature, but the reduction was still incomplete at 1400 °C. Also, a slight amount of $Mg_3B_2O_6$ was formed at 1200 and 1400 °C.

This brief review shows that synthesis of ZrB_2 with a magnesiothermic reduction step is a promising approach because it utilizes chemical energy that is released by exothermic reactions and because MgO can be easily removed from the products by mild acid leaching. The mechanism of magnesiothermic SHS includes exothermic reactions of Mg with the boron source and, at higher temperatures, with zirconia. The latter reaction generates Zr, which immediately reacts with already formed B, generating a lot of heat. Although the total released heat is less than in the case of synthesis from elements (i.e., Zr and B), mechanical activation facilitates ignition and enables a self-sustained combustion. However, incomplete conversion of oxides/acids to boride is a major problem in the magnesiothermic reduction methods.

The present paper focuses on the improvement of the oxide-to-boride conversion in magnesiothermic SHS of ZrB_2. Our thermodynamic calculations, conducted using THERMO (version 4.3) software [47] at 1 atm, have shown that the adiabatic flame

temperature of the stoichiometric (Eq. 2) ZrO_2–B_2O_3–Mg system is equal to 2369 K (2096 °C) and the equilibrium combustion products contain unreacted Mg vapor and oxides of zirconium and boron. An increase in Mg concentration above the stoichiometry decreases the temperature and the oxide concentrations. At 77 mol% Mg (the stoichiometry is 71.4 mol% Mg), the adiabatic flame temperature is 2130 K (1857 °C), and the theoretical oxide-to-boride conversion is 100% (see Figs. S1 and S2 in Supplementary Information). Also, the decrease in the temperature and the increase in the conversion can be achieved with inert diluents.

In practice, however, there is a loss of magnesium at significantly lower temperatures (the boiling point of Mg is 1093 °C at 1 atm [27]) and this is commonly considered as the primary cause for incomplete conversion in magnesiothermic reduction. To decrease the Mg loss, it would be beneficial to lower the combustion temperature below the boiling point of Mg, but this may make the mixture uncombustible. In other words, it is hard to maintain a relatively low combustion temperature and simultaneously ensure a self-sustained combustion. Mechanical activation could help with solving this problem.

The combustion temperature can be decreased by adding an inert diluent [25]. According to the SHS literature, the final product is commonly used for this purpose [18, 19]. In the considered combustion process, the final product is a mixture of ZrB_2 and MgO. Obviously, it is sufficient to add only one of these two compounds, for example, MgO.

Another potentially useful additive is sodium chloride (NaCl). An additional advantage of this additive is the fact that NaCl can also be used in the mechanical activation step as it helps mill relatively soft materials, such as Al and Mg, and can easily be removed from the final product [50]. Furthermore, NaCl decreases the product particle size [28], leading to better properties.

The combustion temperature can also be decreased by adding more Mg. Note that adding a small amount of Mg alone may not help. For example, if there is a loss of Mg from the stoichiometric mixture, adding the same amount will increase the temperature. Therefore, the amount of excess Mg should be significantly large to make the mixture Mg-rich. This is not desired from the practical standpoint as Mg is more expensive than MgO or NaCl. However, since the addition of an inert diluent may not completely prevent the loss of Mg, it may be necessary to add some amount of Mg in addition to the inert diluent.

Experimental

Zirconium (IV) oxide (ZrO_2, − 325 mesh, 99.7% pure, Alfa Aesar), boron trioxide (B_2O_3, 99.8% pure, Sigma-Aldrich), magnesium (Mg, − 325 mesh, 99.8% pure, Sigma-Aldrich), magnesium oxide (MgO, − 325 mesh, ≥ 99% pure, Sigma-Aldrich), and sodium chloride (NaCl, 99% pure, Sigma-Aldrich) powders were mixed in a three-dimensional inversion kinematics tumbler mixer (Inversina 2L, Bioengineering). The reactants were mixed at ZrO_2/B_2O_3/Mg stoichiometry (Eq. 2, 1:1:5 mol ratio) and with 20% excess magnesium (1:1:6 mol ratio). In both cases, the concentrations of inert diluents (MgO and NaCl) were varied over wide ranges. The mixtures were mechanically activated in a planetary ball mill (Fritsch Pulverisette 7 Premium Line) using zirconia-coated grinding bowls and zirconia grinding balls (diameter 3 mm). The total mass of powders to mill was 15 g and the balls-mixture mass ratio was 20:3. To avoid oxidation of Mg, the mixing and milling processes were conducted in an ultra-high-purity argon environment. The milling speed was 1000 rpm, and four total milling times were used: 1, 5, 10, and 30 min. To minimize temperature increase and prevent reactions during milling, the process was separated into cycles with 1-min milling periods and 60-min cooling pauses.

The mechanically activated mixtures were compacted into 4-g cylindrical pellets (diameter 13 mm) in a pressing die using a uniaxial hydraulic press. The pellets had different heights, 13–23 mm, because of different densities of the tested mixtures. Pressing was conducted at 150 MPa with a holding time of 5 min. Booster pellets (diameter 13 mm, mass 1 g) of Ti/B mixture (1:2 mol ratio) were compacted at the same pressing parameters. The booster pellets were used to ensure close ignition parameters in all experiments. Heating directly by a hot wire may lead to an undesired variation of the ignition energy, but identical booster pellets provide identical amounts of heat. Estimates show that the heat transferred from the hot wire in the conducted experiments is much less than the heat released by the booster pellet (the formation enthalpy of TiB_2 is 4.02 kJ/g [27]).

The combustion process was performed inside a windowed steel chamber (diameter 30 cm, height 40 cm), connected to a compressed argon (ultra-high purity) cylinder and a vacuum pump. All experiments were conducted in an argon environment at 1 atm. To minimize residual air in the environment, the reaction chamber was evacuated and filled with argon three times. The pellet, installed vertically on a piece of 3-mm-thick thermal paper (Fiberfrax), was ignited at the top by a tungsten wire heated with a DC power supply (Mastech HY3050EX).

Digital video recording (Sony XCD-SX90CR) was used for observation. In several experiments, the temperature in the middle of the pellet was measured with a thermocouple. Also, in several other experiments, two thermocouples with hot junctions positioned 10 mm apart at the pellet axis were installed, which allowed for the combustion front velocity to be determined from the thermocouple measurements. The measurements were conducted with WRe5%/WRe26% thermocouples (type C, wire diameter 76 μm, Omega Engineering). Each thermocouple was located in a two-channel ceramic insulator (outer diameter 0.8 mm, Omegatite 450, Omega Engineering). To install the thermocouples, 6.5-mm-deep channels were drilled perpendicularly to the pellet axis.

After the SHS process, the obtained product pellet was separated from the titanium diboride product of the booster pellet combustion and ground into a powder using a mortar and pestle. MgO and NaCl in the products were leached in 200 mL of 1 M HCl solution. The amount of acid was by at least 60% larger than what is needed for fully removing MgO according to the reaction stoichiometry. The dissolution process was carried out in an Erlenmeyer flask with a mechanical stirrer at atmospheric pressure and room temperature for 2 h. The remaining solid products were separated from the acid using a paper filter. Then, the solid products were washed in deionized water and dried at room temperature for 24 h.

Particle size distributions of the as-received powders and milled mixtures were determined with a laser diffraction particle size analyzer (Microtrac Bluewave). To avoid oxidation or dissolution of the powders, isopropyl alcohol was used as the sample carrier.

Compositions of the milled mixtures and combustion products before and after leaching were studied using powder X-ray diffraction analysis (Bruker D8 Discover XRD, Cu K-alpha 1, 0.154 nm). The scan was conducted in a 2θ range of 20°–60° with a scan speed of 5 °/min and a step size of 0.02°. The products obtained from the mixtures with 0 and 20% excess Mg and different NaCl contents were also subjected to quantitative XRD analysis using the Rietveld and Scherrer methods with Bruker TOPAS 4.2 software based on the data obtained with a Rigaku MiniFlex II diffractometer over the same scan range with a scan speed of 1 °C/min and a step size of 0.01°.

The morphology of the leached powders was studied using a scanning electron microscope (SEM, Hitachi S-480) with a secondary electrons detector. The samples were compacted into pellets (diameter 6.5 mm) and mounted in carbon conductive tabs (diameter 12 mm). The accelerating voltage was varied from 10 to 25 kV.

Results and discussion

Mechanical activation

The particle size distributions of the powders were measured before and after milling. The initial ZrO_2 powder had a bimodal distribution with a mean volume diameter of 15.3 μm, while B_2O_3, Mg, MgO, and NaCl had unimodal particle size distributions with the mean volume diameters being equal to 144, 15.9, 4.5, and 432.3 μm, respectively. After 1-min milling, unimodal particle size distributions were observed in all mixtures. An increase in the milling time decreased the particle size. For example, increasing the milling time from 1 to 10 min decreased the mean volume diameter from 42 to 21 μm in $ZrO_2/B_2O_3/Mg/MgO$ mixtures (40 wt% MgO) and from 31 to 23 μm in $ZrO_2/B_2O_3/Mg/NaCl$ mixtures (40 wt% NaCl). Figures S3–S11 in Supplementary Information show the particle size distributions of the as-received powders and of the aforementioned milled mixtures.

In MASHS, in contrast with mechanical alloying or MSR, milling is conducted for a short period of time, with no significant reaction inside the grinding bowl. Figure 1 shows the XRD patterns of the stoichiometric $ZrO_2/B_2O_3/Mg$ (1:1:5 mol ratio, Eq. 2) mixture before and after 1-min milling. The XRD pattern of the milled mixture does not show any traces of MgO

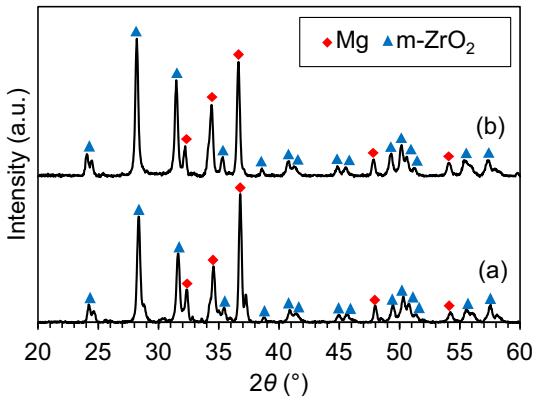

Figure 1 XRD patterns of stoichiometric $ZrO_2/B_2O_3/Mg$ mixture **a** before and **b** after 1-min milling.

or ZrB_2, i.e., no apparent reaction took place during milling. The detected changes in the intensities of magnesium crystal planes (202) and (101), located at $2\theta = 34.4°$ and $2\theta = 36.6°$, respectively, were possibly caused by changes in the preferential crystal orientation of Mg after milling. Longer milling times were used only for mixtures with diluents. The XRD patterns of the milled powders have not revealed any reactions (see Fig. S12 in Supplementary Information).

During milling with no diluent, or with added NaCl or MgO, a portion of the material stuck to the grinding balls and the interior surface of the bowl and thus could not easily be recovered and used for the experiments. Figure 2 shows the percentage of mixture stuck during milling versus diluent concentration. It is seen that with no diluent, 24% of the mixture was stuck. At 25–40 wt% MgO, the stuck mass was still significant, 14–21%. In contrast, by adding only 10 wt% NaCl the amount of stuck mixture dropped to about 5%. Additionally, for longer total milling times, the amount of stuck mixture stagnates around 5% when the NaCl content is in the range from 40 to 55 wt%.

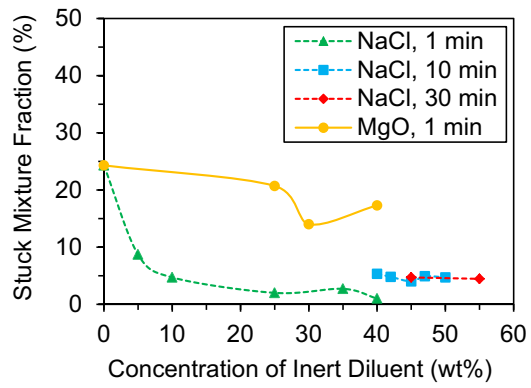

Figure 2 Percentage of mixture that is stuck to the grinding media for different diluents and milling times versus the diluent concentration in the initial mixture.

SHS process for stoichiometric $ZrO_2/B_2O_3/Mg$ mixture

The stoichiometric $ZrO_2/B_2O_3/Mg$ mixture was not ignitable without a preceding milling step, but milling for 1 min enabled the ignition and a self-sustained combustion. Video 1 in Supplementary Information shows the combustion process of the milled stoichiometric $ZrO_2/B_2O_3/Mg$ mixture. The observed vigorous combustion was accompanied by the formation of a layered structure of the product. Analysis of this product revealed that it was fragile and porous.

Figure 3 shows the thermocouple record at the center of the pellet for the same combustion process. Since the voltage–temperature characteristic of a C-type thermocouple is strongly nonlinear [51], the plot shows the voltage, while dashed gridlines indicate temperatures for reference. The time variation of temperature exhibits a sharp temperature rise followed by a gradual decrease due to cooling. The maximum recorded temperature is 1725 °C, which is by 372 °C lower than the adiabatic flame temperature (2097 °C) for this mixture. This temperature difference could be attributed to heat losses and incomplete combustion.

Figure 4 shows the XRD pattern of the stoichiometric $ZrO_2/B_2O_3/Mg$ mixture after combustion. It is seen that the dominant phases are ZrB_2 and MgO, with c-ZrO_2 and $Mg_3(BO_3)_2$ impurities. Note that

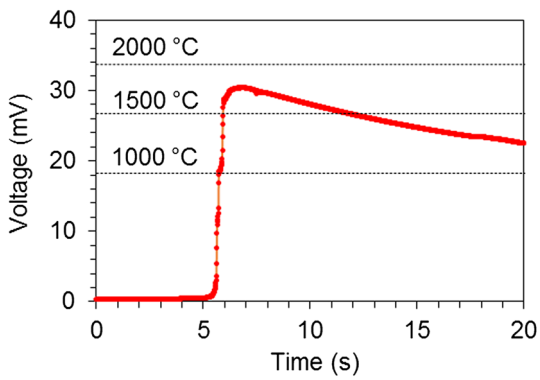

Figure 3 Thermocouple signal for stoichiometric $ZrO_2/B_2O_3/Mg$ mixture. Time zero was selected arbitrarily.

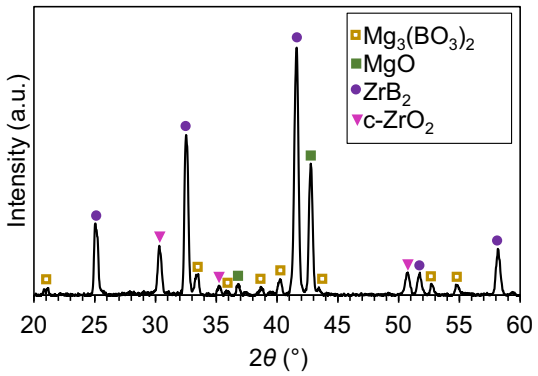

Figure 4 XRD pattern of the stoichiometric $ZrO_2/B_2O_3/Mg$ mixture after combustion.

before combustion, ZrO_2 in the mixture was in its stable room-temperature phase (monoclinic zirconia, m-ZrO_2), but after combustion, the metastable high-temperature phase (cubic zirconia, c-ZrO_2) appeared. The presence of the metastable phase is explained by the fact that it forms a solid solution with MgO at temperatures higher than about 1400 °C [52]. Magnesia-stabilized zirconia normally contains around 10 mol% MgO, but that value can vary. Although there is unreacted ZrO_2, the XRD pattern of the combustion products does not show unreacted Mg, which indicates the loss of Mg as a result of higher combustion temperature than the boiling point of Mg.

Figure 5 shows the XRD pattern of the products after leaching. It is seen that MgO almost disappeared, but the peaks of $Mg_3(BO_3)_2$ phase remained virtually the same.

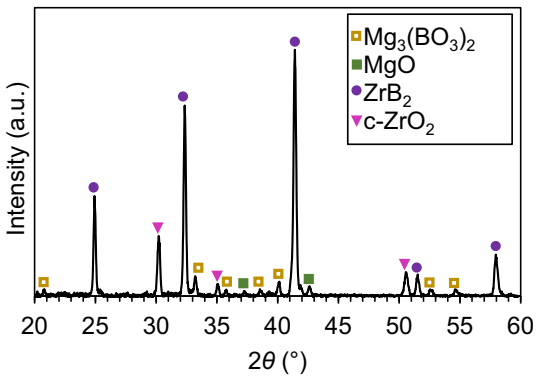

Figure 5 XRD pattern of the stoichiometric $ZrO_2/B_2O_3/Mg$ mixture after combustion and leaching.

Effect of MgO additive on magnesiothermic SHS of ZrB_2

Combustion experiments were conducted with $ZrO_2/B_2O_3/Mg/MgO$ mixtures where the reactants were mixed according to the stoichiometry (Eq. 2) and MgO concentration was varied from 20 to 40 wt%. Mechanical activation was conducted at two total milling times: 1 and 10 min. In general, it was easier to ignite the 10-min milled $ZrO_2/B_2O_3/Mg/MgO$ mixtures than the 1-min milled ones. Figure 6 shows the combustion images for the mixture with 30% MgO, milled for 1 min, and for the mixture with 40% MgO, milled for 10 min (see also Video 2 and Video 3, respectively, in Supplementary Information). No oscillations in the combustion front propagation were observed. However, 30 wt% MgO was the maximum concentration of this diluent that allowed a self-sustained reaction for mixtures that were milled for 1 min, whereas mixtures that were milled for 10 min were easily ignited even at 40 wt% MgO and they emitted more light during combustion. Similarly to the observations for combustion of stoichiometric mixtures without any inert diluent, the combustion products were fragile and porous.

Figure 7 shows the XRD pattern of $ZrO_2/B_2O_3/Mg/MgO$ mixture (40 wt% MgO) after combustion. It is seen that ZrB_2 and MgO are the dominant phases, but ZrO_2 and $Mg_3(BO_3)_2$ are also present in the products. Note that because of the lower combustion

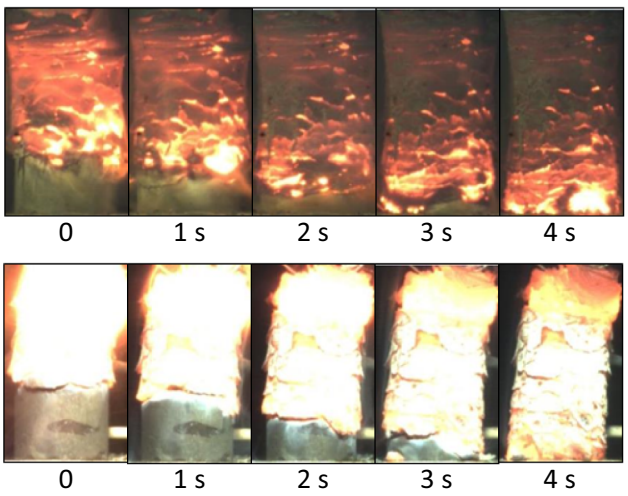

Figure 6 Combustion of $ZrO_2/B_2O_3/Mg/MgO$ mixtures at (top) 30 wt% MgO and 1-min milling and (bottom) 40 wt% MgO and 10-min milling. Time zero was selected 4 s before the end of the combustion process.

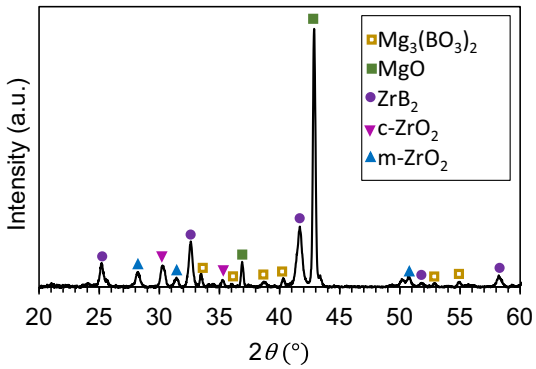

Figure 7 XRD pattern of $ZrO_2/B_2O_3/Mg/MgO$ mixture (40 wt% MgO) after combustion.

temperatures in the mixtures with MgO, ZrO_2 was observed in two phases, monoclinic and cubic.

To explore the effect of MgO additive on the conversion of ZrO_2 to ZrB_2, the XRD patterns of the combustion products (before leaching) were analyzed. The highest peaks for m-ZrO_2 (plane ($\bar{1}$ 11), $2\theta = 28.2°$), c-ZrO_2 (plane (111), $2\theta = 30.5°$), and ZrB_2 (plane (101), $2\theta = 41.6°$) phases were considered in the analysis. The intensity ratios of m-ZrO_2 and c-ZrO_2 peaks to ZrB_2 peak were determined and served for characterization of the oxide-to-boride conversion degree (a zero ratio corresponds to full conversion).

Figure 8 shows the peak intensity ratios of the two ZrO_2 phases in the combustion products versus MgO concentration in the initial mixture. It is seen that at 0 wt% MgO, monoclinic zirconia is absent, but the ratio for cubic zirconia is about 0.2. Note that 0 wt% MgO corresponds to the XRD pattern shown in Fig. 4. With increasing MgO content, the peak

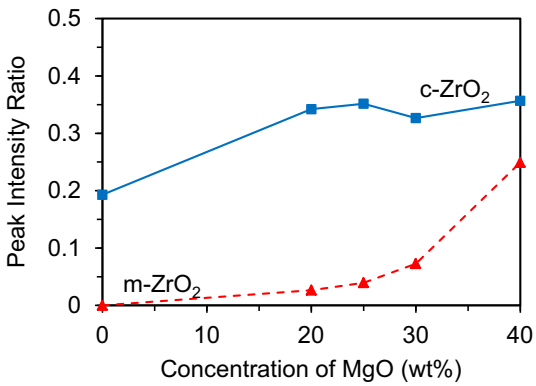

Figure 8 Intensity ratios of m-ZrO_2 and c-ZrO_2 peaks to ZrB_2 peak in the combustion products versus MgO concentration in the initial mixture.

intensity ratio for m-ZrO_2 increases exponentially. The ratio for cubic ZrO_2 significantly increases with increasing MgO concentration from 0 to 20 wt%, but changes only slightly with further increase. In general, these results clearly indicate that MgO has an adverse effect on the conversion of oxides to borides. For this reason, leaching of the products obtained from these mixtures was not conducted.

Effect of NaCl additive on magnesiothermic SHS of ZrB_2

Combustion experiments were conducted with $ZrO_2/B_2O_3/Mg/NaCl$ mixtures where the reactants were mixed according to the stoichiometry (Eq. 2) and NaCl concentration was varied from 5 to 55 wt%. After milling for 1 min, the mixtures with up to 35 wt% NaCl became ignitable, but the mixtures with 35–50 wt% NaCl required 10 min of milling for combustion to occur. To ignite mixtures with 55 wt% NaCl, the required milling time was 30 min.

Figure 9 shows the combustion process for $ZrO_2/B_2O_3/Mg/NaCl$ mixtures at 40 and 47 wt% NaCl, milled for 10 min (see also Videos 4 and 5 in Supplementary Information). It is seen that at a higher NaCl content, the combustion front propagates slower and emits less light. In contrast with the results for mixtures with no inert diluent and for those with MgO, the products were dense and hard. This can be explained by melting of NaCl (melting

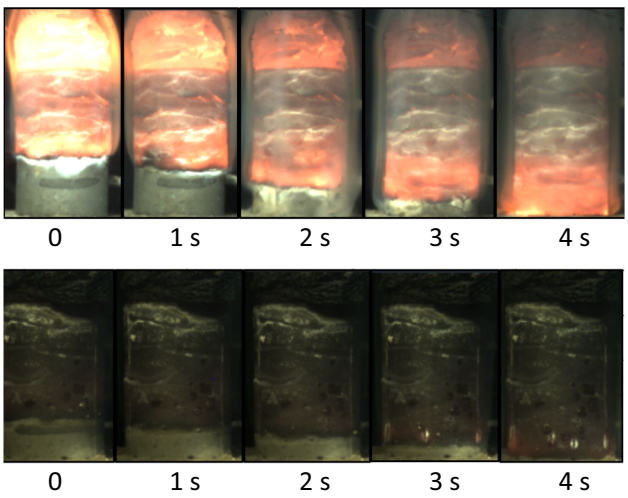

Figure 9 Combustion of $ZrO_2/B_2O_3/Mg/NaCl$ mixtures at (top) 40 and (bottom) 47 wt% NaCl, milled for 10 min. Time zero was selected arbitrarily.

point: 801 °C [27]) during combustion and its subsequent solidification during cooling.

The observed deceleration of the front propagation with increasing NaCl concentration is explained by the decrease in the heat release and hence in the combustion temperature. Figure 10 shows the signals of two C-type thermocouples, located 10 mm apart on the pellet axis, during combustion of $ZrO_2/B_2O_3/Mg/NaCl$ mixture (47 wt% NaCl). It is seen that the maximum temperature for each thermocouple is about 1200 °C, i.e., by over 500 °C lower than the maximum temperature measured during combustion of the stoichiometric mixture with no diluent. For all mixtures, the combustion front velocities were determined using video records, and the obtained values range from 3.2 mm/s for the stoichiometric mixture with no diluent to 0.6 mm/s for the mixture with 55 wt% NaCl. For mixtures with NaCl concentrations of 40–50 wt%, milled for 10 min, the combustion front velocity was also determined from the time lag between the temperature rises of the two thermocouple signals and the results are shown in Fig. S13 in Supplementary Information.

Figures 11 and 12 show the XRD patterns of the products of $ZrO_2/B_2O_3/Mg/NaCl$ mixture (40 wt% NaCl), milled for 10 min, after combustion and leaching, respectively. It is seen that ZrB_2, MgO, and NaCl are the most prominent phases in the combustion products and $Mg_3(BO_3)_2$, m-ZrO_2, and c-ZrO_2 impurities are also present. Leaching fully removed both MgO and NaCl, but traces of $Mg_3(BO_3)_2$ phase remained, along with noticeable amounts of m-ZrO_2 and c-ZrO_2.

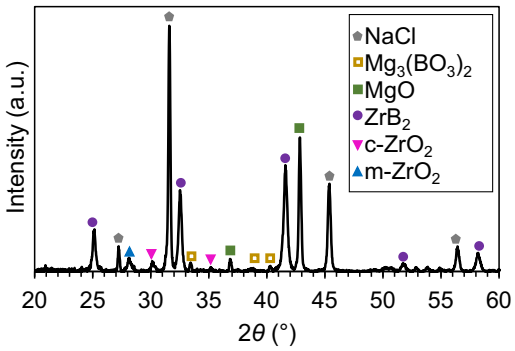

Figure 11 XRD pattern of $ZrO_2/B_2O_3/Mg/NaCl$ mixture (40 wt% NaCl) after combustion.

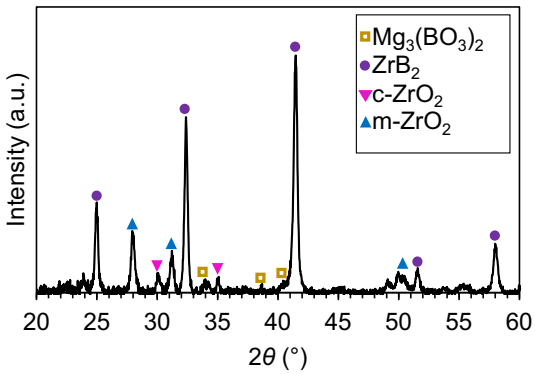

Figure 12 XRD pattern of $ZrO_2/B_2O_3/Mg/NaCl$ mixture (40 wt% NaCl) after combustion and leaching.

The XRD peak ratio analysis was conducted for $ZrO_2/B_2O_3/Mg/NaCl$ mixtures after combustion and after leaching. Figure 13 shows the peak intensity ratios for both ZrO_2 phases with respect to ZrB_2 in the combustion products (before leaching) as well as the maximum measured temperatures versus NaCl concentration in the initial mixture. It is seen

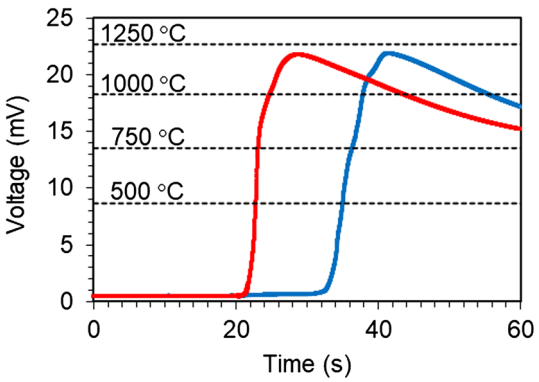

Figure 10 Signals of two thermocouples, located 10 mm apart on the pellet axis, during combustion of $ZrO_2/B_2O_3/Mg/NaCl$ mixture (47 wt% NaCl).

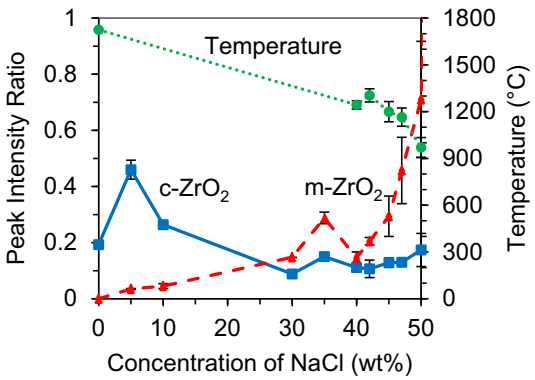

Figure 13 Intensity ratios of m-ZrO_2 and c-ZrO_2 peaks to ZrB_2 peak and maximum temperature versus NaCl concentration in the initial mixture (ZrO_2:B_2O_3:Mg = 1:1:5), after combustion.

that at low concentrations of NaCl, the peak intensity ratio of the cubic ZrO_2 phase is significantly higher than that of monoclinic ZrO_2, whereas the situation is inverse at higher concentrations of NaCl.

Since the increase in NaCl content decreases the combustion temperature, it makes sense to discuss these observations based on thermodynamics. The ZrO_2–MgO phase diagram [52] shows that with no MgO the monoclinic ZrO_2 is stable at temperatures below about 1000 °C, the tetragonal phase is stable between about 1000 and about 2400 °C, and the cubic phase is stable at higher temperatures. The addition of MgO significantly decreases the low temperature limit for the existence of cubic ZrO_2. MgO also has a stabilizing effect [53], which explains why the cubic phase is not converted to the monoclinic phase in the course of relatively rapid cooling, typical for SHS.

Figure 14 shows the peak ratios of both ZrO_2 phases versus NaCl concentration for the leached products. Comparison with the data for the combustion products presented in Fig. 14 shows that c-ZrO_2 phase intensity remained about the same after leaching, but the values for m-ZrO_2 phase significantly increased. This indicates that apparently ZrB_2 was oxidized during leaching, which correlates with prior observations [54]. The oxidation mechanism during the leaching procedure is unclear. It may involve the formation of metallic Zr (the reaction of ZrB_2 with 6 M HCl solution produced B_6H_6 gas [55]). The formed Zr may be oxidized either by water in the acid solution or by atmospheric oxygen during drying. The latter process was, for example, observed for Al powder after leaching NaCl by water [56].

Figure 15 shows the results of the Rietveld XRD analysis for these mixtures. Specifically, it shows the mass concentrations of cubic and monoclinic phases of ZrO_2 in the leached products as well as the oxygen content, calculated based on these data. It is seen that the Rietveld analysis of ZrO_2 phases has confirmed the conclusions from the analysis based on the peak ratios. It has also provided data for calculating the conversion degree and the oxygen concentration in the products. For example, in the products obtained from the mixture with 30 wt% NaCl, the conversion degree is 80% and the concentration of oxygen is about 12 wt%.

The Scherrer analysis has shown that with increasing NaCl concentration from 0 to 50 wt%, the crystallite size decreases from 223 nm to 18 nm. Scanning electron microscopy has confirmed the significant effect of NaCl on the product size. Figure 16 shows the SEM images of the leached combustion products of stoichiometric $ZrO_2/B_2O_3/Mg$ mixture with (a) no NaCl and (b) 30 wt% NaCl. It is seen that the particles in the leached products of the mixture with 30 wt% NaCl are much smaller than those in the leached products of the mixture with no inert diluent. As noted in the Introduction, the effect of NaCl on particle size was previously reported [28, 57–59] and a smaller particle size usually leads to a lower sintering temperature, which is highly desired.

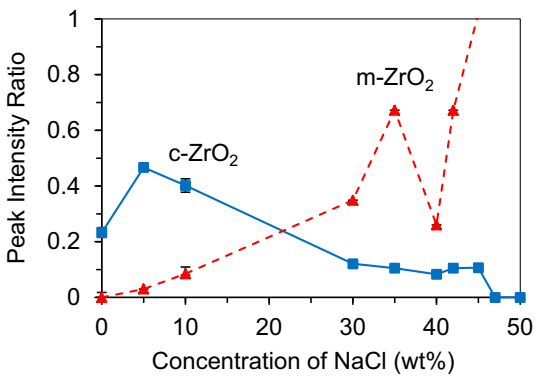

Figure 14 Intensity ratios of m-ZrO_2 and c-ZrO_2 peaks toZrB_2 peak versus NaCl concentration in the initial mixture (ZrO_2:B_2O_3:Mg = 1:1:5), after leaching.

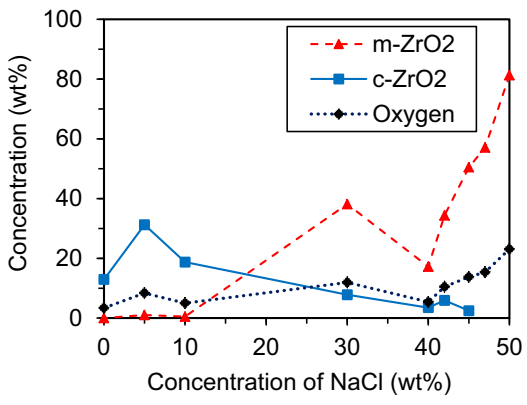

Figure 15 Concentrations of ZrO_2 phases and oxygen content in the products obtained after combustion and leaching stoichiometric $ZrO_2/B_2O_3/Mg$ mixtures with different concentrations of NaCl.

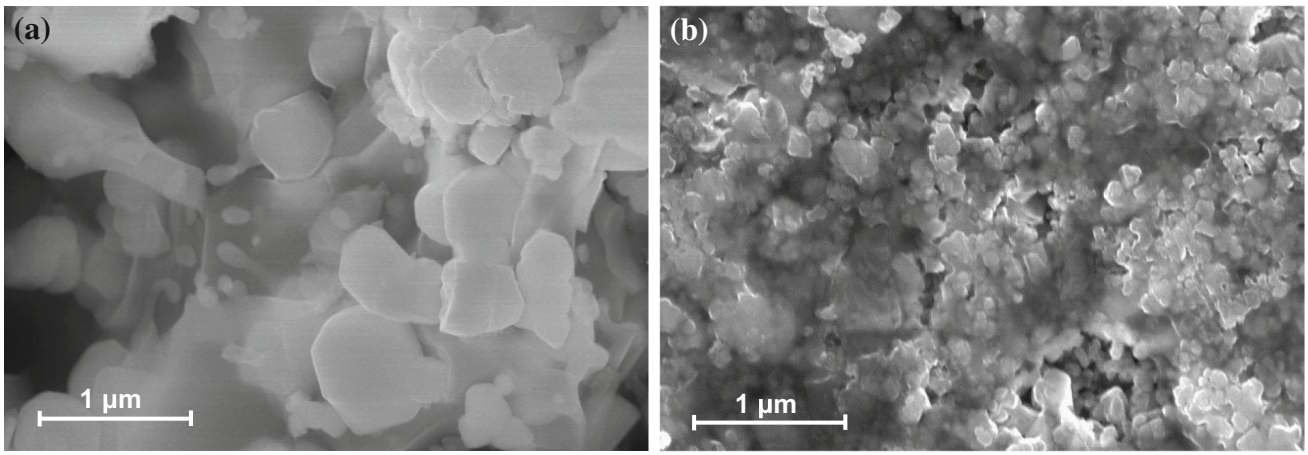

Figure 16 SEM images of the leached combustion products of stoichiometric $ZrO_2/B_2O_3/Mg$ mixture **a** with no NaCl and **b** with 30 wt% NaCl.

Effect of excess Mg on magnesiothermic SHS of ZrB_2

Since the addition of NaCl to the stoichiometric $ZrO_2/B_2O_3/Mg$ mixture did not fully eliminate ZrO_2 in the combustion products, it was suggested that extra Mg could compensate for the lost Mg and reduce the remaining oxides. Combustion experiments were conducted with $ZrO_2/B_2O_3/Mg/NaCl$ mixtures where the amounts of excess Mg and NaCl were varied.

First, experiments were conducted where the concentration of NaCl was fixed at 10 wt% NaCl and the amount of excess Mg was varied. To obtain a stable combustion, it was sufficient to mill the mixture for 1 min. Figure 17 present the peak intensity ratios of the ZrO_2 phases in the combustion products of these mixtures (no leaching). It is seen that the total amount of ZrO_2 significantly decreases with increasing the amount of excess Mg to 20%.

Based on these results, it was decided to select 20% excess Mg for further experiments and investigate the effect of NaCl on the product composition. To ignite the mixtures, 5-min milling was required. Vigorous combustion was observed (see Video 6 in Supplementary Information), similar to that for the stoichiometric mixture with no inert diluents.

Figures 18 and 19 show the XRD patterns of the products for the mixture with 20% excess Mg and 30 wt% NaCl, after combustion and after leaching, respectively. It is seen that MgO and $Mg_3(BO_3)_2$ were fully removed by leaching though traces of monoclinic and cubic phases of ZrO_2 are present in the products.

Figure 20 presents the peak intensity ratios of the ZrO_2 phases in the combustion products (before leaching) and maximum temperatures versus NaCl concentration for the mixtures with 20% excess Mg.

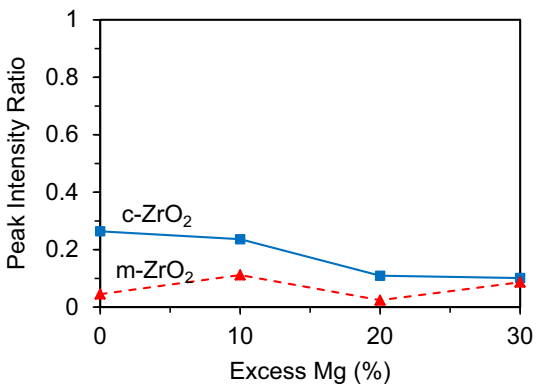

Figure 17 Intensity ratios of m-ZrO_2 and c-ZrO_2 peaks to ZrB_2 peak versus amount of excess Mg in the initial mixture with 10 wt% NaCl, after combustion.

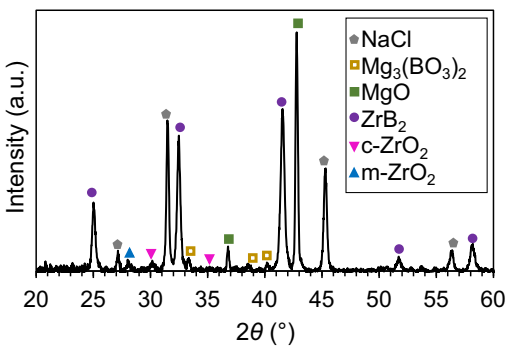

Figure 18 XRD pattern of $ZrO_2/B_2O_3/Mg/NaCl$ mixture with 20% excess Mg and 30 wt% NaCl after combustion.

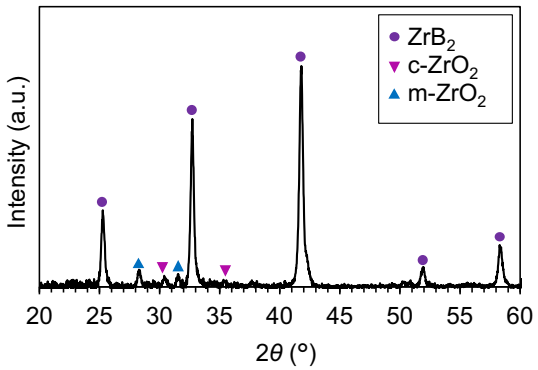

Figure 19 XRD pattern of $ZrO_2/B_2O_3/Mg/NaCl$ mixture with 20% excess Mg and 30 wt% NaCl after leaching.

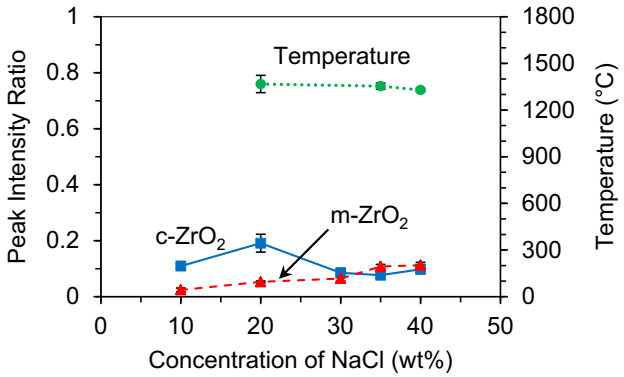

Figure 20 Intensity ratios of m-ZrO_2 and c-ZrO_2 peaks to ZrB_2 peak and maximum temperature versus NaCl concentration in the initial mixture (20% excess Mg) after combustion.

Comparison with Fig. 13 shows that the maximum temperatures during combustion of mixtures with 20% excess Mg were approximately the same as for the stoichiometric mixtures. The relationships between the peak intensity ratios for cubic and monoclinic phases of ZrO_2 also remained similar to those for the stoichiometric mixture, but, in general, the peak ratios of ZrO_2 phases were lower in the experiments with 20% excess Mg. The lowest sum of the two peak ratios was observed at 30 wt% NaCl.

Figure 21 shows the results for the products obtained by combustion of mixtures with 20% excess Mg, after leaching. Comparison with the data in Fig. 20 shows that, like in the experiments with stoichiometric mixtures, the content of m-ZrO phase increases after leaching, which indicates oxidation of ZrB_2. Leaching, however, does not affect the amount of c-ZrO_2. In general, the conversion was much better than for the stoichiometric mixtures (see Fig. 14).

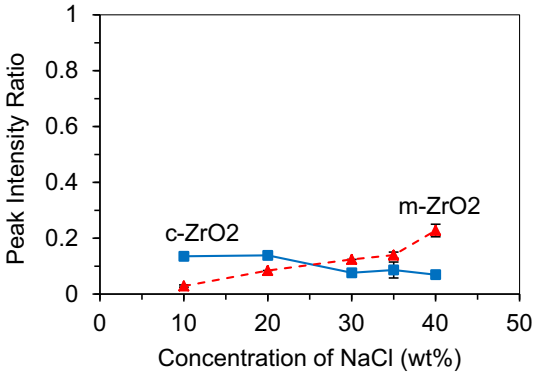

Figure 21 Intensity ratios of m-ZrO_2 and c-ZrO_2 peaks to ZrB_2 peak versus NaCl concentration in the initial mixture with 20% excess Mg, after leaching.

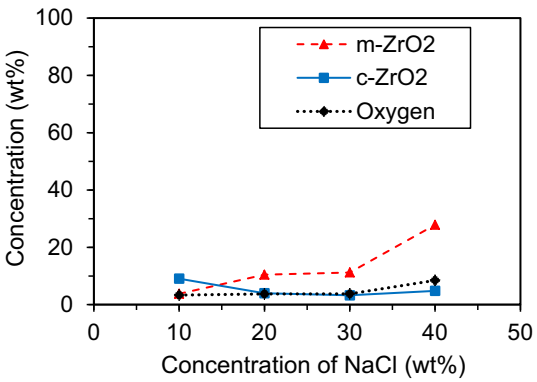

Figure 22 Concentrations of ZrO_2 phases and oxygen content in the products obtained after combustion and leaching of mixtures with 20% excess Mg and different concentrations of NaCl.

Figure 22 shows the results of the Rietveld analysis for the products obtained by combustion of mixtures with 20% excess Mg, after leaching. Like in the case of the stoichiometric mixtures with NaCl diluent, the results for ZrO_2 phases correlates with the analysis based on the peak intensity ratios. The oxygen content is 3.34 wt% at 10 wt% NaCl and 3.75 wt% at 20–30 wt% NaCl; the conversion degree is 88 and 86%, respectively. ZrB_2 powders with similar amounts of oxygen were densified using pressureless sintering with boron carbide and/or carbon as sintering aids [38].

Based on the results presented in this section, it was concluded that the mixture with 20% excess Mg and 30 wt% NaCl is promising. According to the Scherrer analysis, the crystallite size of the products obtained by combustion of this mixture after leaching is 40 nm. This value is comparable with prior results

on magnesiothermic synthesis of ZrB2 (75 nm [43], 25 nm [12]).

Figure 23 shows an SEM image of the leached combustion products of $ZrO_2/B_2O_3/Mg/NaCl$ mixture with 20% excess Mg and 30 wt% NaCl. It is seen that the obtained ZrB_2 powder consists of nanoscale polycrystalline particles. Note that polycrystalline particles sinter more rapidly than single-crystal particles [60]. It should also be noted that the decrease in the particle size due to the addition of NaCl may also have a negative consequence, viz., the faster oxidation of smaller ZrB_2 particles during leaching and drying.

Conclusions

The addition of MgO to the stoichiometric $ZrO_2/B_2O_3/Mg$ mixture cannot decrease sticking of mixture to the bowl and grinding media during high-energy ball milling. The MgO addition also increases the amount of ZrO_2 (both monoclinic and cubic phases) in the combustion products.

In contrast, the addition of NaCl dramatically decreases the amount of mixture stuck during mechanical activation. Milling the stoichiometric $ZrO_2/B_2O_3/Mg$ mixture with NaCl for 1 min at a rotation speed of 1000 rpm enables a self-sustained combustion though pulsations of the front propagation are observed. Increasing the milling time to 10 min ensures a steady propagation. The combustion products include ZrB_2 and MgO as dominant phases, but ZrO_2 and $Mg_3(BO_3)_2$ are also present. The increase in NaCl concentration from 5 to 50% increases the amount of monoclinic zirconia, but decreases the amount of cubic zirconia in the products, which correlates with the decrease in the combustion temperature and with the ZrO_2–MgO phase diagram.

MASHS of mixtures with excess Mg and NaCl diluent produces promising materials. The addition of 20% excess Mg decreases the amount of ZrO_2 in the combustion products, while the addition of NaCl decreases the particle size of the products, which is beneficial for sintering. Leaching the combustion products of the mixture with 20% excess Mg and 30 wt% NaCl in 1 M HCl solution fully removes MgO and $Mg_3(BO_3)_2$ though the monoclinic and cubic phases of ZrO_2 are still present in the products. In the products obtained by combustion and leaching of the mixtures with 20% excess Mg and 10–30 wt% NaCl, the oxygen content is below 4 wt%.

Summarizing, the addition of 20% excess Mg and 30 wt% NaCl to the stoichiometric $ZrO_2/B_2O_3/Mg$ mixture ensures effective mechanical activation, a steady self-sustained combustion, and a relatively small amount of zirconia in the combustion products. The obtained ZrB_2 powder consists of nanoscale polycrystalline particles.

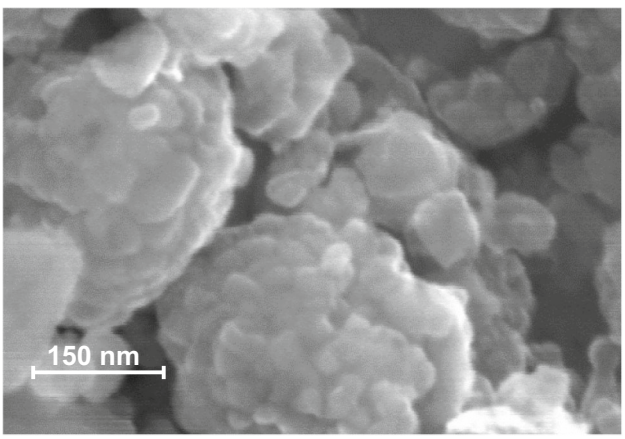

Figure 23 SEM image of the leached combustion products of $ZrO_2/B_2O_3/Mg/NaCl$ mixture with 20% excess Mg and 30 wt% NaCl.

Disclaimer

Acknowledgements

This material is based upon work supported by the Department of Energy, National Energy Technology Laboratory under Award Number DE-FE0026333 (Program Manager: Jason C. Hissam).

Electronic supplementary material: The online version of this article (https://doi.org/10.1007/s10853-018-2460-8) contains supplementary material, which is available to authorized users.

References

[1] Fahrenholtz WG, Hilmas GE, Talmy IG, Zaykoski JA (2007) Refractory diborides of zirconium and hafnium. J Am Ceram Soc 90:1347–1364. https://doi.org/10.1111/j.1551-2916.2007.01583.x

[2] Shein IR, Ivanovskii AL (2002) Band structure of ZrB_2, VB_2, NbB_2, and TaB_2 hexagonal diborides: comparison with superconducting MgB_2. Phys Solid State 44:1833–1839. https://doi.org/10.1134/1.1514768

[3] Zhong MM, Kuang XY, Wang ZH et al (2013) Phase stability, physical properties, and hardness of transition-metal diborides MB_2 (M = Tc, W, Re, and Os): first-principles investigations. J Phys Chem C 117:10643–10652. https://doi.org/10.1021/jp400204c

[4] Vajeeston P, Ravindran P, Ravi C, Asokamani R (2001) Electronic structure, bonding, and ground-state properties of AlB_2-type transition-metal diborides. Phys Rev B Condens Matter Mater Phys 63:1–12. https://doi.org/10.1103/PhysRevB.63.045115

[5] Shveikin GP, Ivanovskii AL (1994) The chemical bonding and electronic properties of metal borides. Russ Chem Rev 63:711–734. https://doi.org/10.1070/RC1994v063n09ABEH000114

[6] Levine SR, Opila EJ, Halbig MC et al (2002) Evaluation of ultra-high temperature ceramics foraeropropulsion use. J Eur Ceram Soc 22:2757–2767. https://doi.org/10.1016/S0955-2219(02)00140-1

[7] Gasch M, Ellerby D, Irby E et al (2004) Processing, properties and arc jet oxidation of hafnium diboride/silicon carbide ultra high temperature ceramics. J Mater Sci 39:5925–5937. https://doi.org/10.1023/B:JMSC.0000041689.90456.af

[8] Sitler SJ, Raja KS, Charit I (2017) Hot corrosion behavior of ZrB_2–HfB_2 solid solutions in KCl and K_2SO_4 at 1500 °C. Ceram Int 43:17071–17085. https://doi.org/10.1016/j.ceramint.2017.09.122

[9] Sonber JK, Suri AK (2011) Synthesis and consolidation of zirconium diboride: review. Adv Appl Ceram 110:321–334. https://doi.org/10.1179/1743676111Y.0000000008

[10] Jalaly M, Tamizifar M, Bafghi MS, Gotor FJ (2013) Mechanochemical synthesis of ZrB_2–SiC–ZrC nanocomposite powder by metallothermic reduction of zircon. J Alloys Compd 581:782–787. https://doi.org/10.1016/j.jallcom.2013.07.142

[11] Jalaly M, Bafghi MS, Tamizifar M, Gotor FJ (2014) The role of boron oxide and carbon amounts in the mechanosynthesis of ZrB_2–SiC–ZrC nanocomposite via a self-sustaining reaction in the zircon/magnesium/boron oxide/graphite system. J Alloys Compd 598:113–119. https://doi.org/10.1016/j.jallcom.2014.02.033

[12] Khanra AK, Pathak LC, Mishra SK, Godkhindi MM (2003) Self-propagating-high-temperature synthesis (SHS) of ultrafine ZrB_2 powder. J Mater Sci Lett 22:1189–1191. https://doi.org/10.1023/A:1025336230885

[13] Khanra AK, Pathak LC, Godkhindi MM (2008) Double SHS of ZrB_2 powder. J Mater Process Technol 202:386–390. https://doi.org/10.1016/j.jmatprotec.2007.09.007

[14] Akgün B, Çamurlu HE, Topkaya Y, Sevinç N (2011) Mechanochemical and volume combustion synthesis of ZrB_2. Int J Refract Met Hard Mater 29:601–607. https://doi.org/10.1016/j.ijrmhm.2011.04.005

[15] Millet P, Hwang T (1996) Preparation of TiB_2 and ZrB_2 influence of a mechano-chemical treatment on the borothermic reduction of titania and zirconia. J Mater Sci 31:351–355. https://doi.org/10.1007/BF01139151

[16] Sonber JK, Murthy TSRC, Subramanian C et al (2011) Investigations on synthesis of ZrB_2 and development of new composites with HfB_2 and $TiSi_2$. Int J Refract Met Hard Mater 29:21–30. https://doi.org/10.1016/J.IJRMHM.2010.06.007

[17] Mishra SK, Das S, Pathak LC (2004) Defect structures in zirconium diboride powder prepared by self-propagating high-temperature synthesis. Mater Sci Eng A 364:249–255. https://doi.org/10.1016/j.msea.2003.08.021

[18] Varma A, Rogachev AS, Mukasyan AS, Hwang S (1998) Combustion synthesis of advanced materials: principles and applications. Adv Chem Eng 24:79–226. https://doi.org/10.1016/S0065-2377(08)60093-9

[19] Moore JJ, Feng HJ (1995) Combustion synthesis of advanced materials: part I. Reaction parameters. Prog Mater Sci 39:243–273. https://doi.org/10.1016/0079-6425(94)00011-5

[20] Moore JJ, Feng HJ (1995) Combustion synthesis of advanced materials: part II. Classification, applications and modelling. Prog Mater Sci 39:275–316. https://doi.org/10.1016/0079-6425(94)00012-3

[21] Morsi K (2012) The diversity of combustion synthesis processing: a review. J Mater Sci 47:68–92. https://doi.org/10.1007/s10853-011-5926-5

[22] Esparza AA, Shafirovich E (2016) Mechanically activated combustion synthesis of molybdenum borosilicides for ultrahigh-temperature structural applications. J Alloys Compd 670:297–305

[23] Delgado A, Cordova S, Shafirovich E (2015) Thermite reactions with oxides of iron and silicon during combustion of magnesium with lunar and Martian regolith simulants. Combust Flame 162:3333–3340. https://doi.org/10.1016/j.combustflame.2015.05.024

[24] Delgado A, Cordova S, Lopez I et al (2016) Mechanically activated combustion synthesis and shockwave consolidation of magnesium silicide. J Alloys Compd 658:422–429. https://doi.org/10.1016/j.jallcom.2015.10.231

[25] Levashov EA, Mukasyan AS, Rogachev AS, Shtansky DV (2017) Self-propagating high-temperature synthesis of advanced materials and coatings. Int Mater Rev 62:203–239. https://doi.org/10.1080/09506608.2016.1243291

[26] Borovinskaya IP, Merzhanov AG, Novikov NP, Filonenko AK (1974) Gasless combustion of mixtures of powdered transition metals with boron. Combust Explos Shock Waves 10:2–10. https://doi.org/10.1007/BF01463777

[27] Chase MW (1998) NIST-JANAF thermochemical tables, 4th edn. Journal of physical and chemical reference data, Monograph 9 (Part I and Part II)

[28] Çamurlu HE, Maglia F (2009) Preparation of nano-size ZrB_2 powder by self-propagating high-temperature synthesis. J Eur Ceram Soc 29:1501–1506. https://doi.org/10.1016/j.jeurceramsoc.2008.09.006

[29] Meekins BH, Lin YC, Manser JS et al (2013) Photoactive porous silicon nanopowder. ACS Appl Mater Interfaces 5:2943–2951. https://doi.org/10.1021/am3031745

[30] Borovinskaya IP, Barinova TV, Vershinnikov VI, Ignat'eva TI (2010) SHS of ultrafine and nanosized refractory powders: an autoreview. Int J Self Prop High Temp Synth 19:114–119. https://doi.org/10.3103/S1061386210020068

[31] Alkan M, Sonmez MS, Derin B, Yücel O (2012) Effect of initial composition on boron carbide production by SHS process followed by acid leaching. Solid State Sci 14:1688–1691. https://doi.org/10.1016/j.solidstatesciences.2012.07.004

[32] Hoseinpur A, Sh M, Vahdati J et al (2015) A mechanistic study on the production of nanosized Mo in microwave assisted combustive reduction of MoO_3 by Zn. Int J Refract Metals Hard Mater 50:191–196. https://doi.org/10.1016/j.ijrmhm.2015.01.012

[33] Jiang G, Xu J, Zhuang H, Li W (2011) Fabrication of B_4C from $Na_2B_4O_7$+Mg+C by SHS method. Ceram Int 37:1689–1691. https://doi.org/10.1016/j.ceramint.2010.10.007

[34] Guojian J, Jiayue X, Hanrui Z, Wenlan L (2009) Combustion of $Na_2B_4O_7$+Mg+C to synthesis B_4C powders. J Nucl Mater 393:487–491. https://doi.org/10.1016/j.jnucmat.2009.07.008

[35] Jamal Abbasi B, Zakeri M, Tayebifard SA (2014) High frequency induction heated sintering of nanostructured Al_2O_3–ZrB_2composite produced by MASHS technique. Ceram Int 40:9217–9224. https://doi.org/10.1016/j.ceramint.2014.01.141

[36] Deris L, Sharafi S, Akbari GH (2014) Effect of milling speed on mechanical activation of Al/ZrO_2/H_3BO_3 system to prepare Al_2O_3–ZrB_2 composite powder. J Therm Anal Calorim 115:401–407. https://doi.org/10.1007/s10973-013-3235-8

[37] Sayagués MJ, Avilés MA, Córdoba JM, Gotor FJ (2014) Self-propagating combustion synthesis via an MSR process: an efficient and simple method to prepare (Ti, Zr, Hf)B_2-Al_2O_3 powder nanocomposites. Powder Technol 256:244–250. https://doi.org/10.1016/j.powtec.2014.02.031

[38] Fahrenholtz WG, Hilmas GE, Zhang SC, Zhu S (2008) Pressureless sintering of zirconium diboride: particle size and additive effects. J Am Ceram Soc 91:1398–1404. https://doi.org/10.1111/j.1551-2916.2007.02169.x

[39] Takacs L (2002) Self-sustaining reactions induced by ball milling. Prog Mater Sci 47:355–414. https://doi.org/10.1016/S0079-6425(01)00002-0

[40] Korchagin MA, Grigoreva TF, Bokhonov BB et al (2003) Solid-state combustion in mechanically activated SHS systems. II. Effect of mechanical activation conditions on process parameters and combustion product composition. Combust Explos Shock Waves 39:51–58. https://doi.org/10.1023/A:1022197218749

[41] Riley DP, Kisi EH, Phelan D (2006) SHS of Ti_3SiC_2: ignition temperature depression by mechanical activation. J Eur Ceram Soc 26:1051–1058. https://doi.org/10.1016/j.jeurceramsoc.2004.11.021

[42] Gotor FJ, Achimovicova M, Real C, Balaz P (2013) Influence of the milling parameters on the mechanical work intensity in planetary mills. Powder Technol 233:1–7. https://doi.org/10.1016/j.powtec.2012.08.031

[43] Setoudeh N, Welham NJ (2006) Formation of zirconium diboride (ZrB_2) by room temperature mechanochemical reaction between ZrO_2, B_2O_3 and Mg. J Alloys Compd 420:225–228. https://doi.org/10.1016/j.jallcom.2005.07.083

[44] Nishiyama K, Nakamur T, Utsumi S et al (2009) Preparation of ultrafine boride powders by metallothermic reduction method. J Phys Conf Ser 176:012043. https://doi.org/10.1088/1742-6596/176/1/012043

[45] Jalaly M, Bafghi MS, Tamizifar M, Gotor FJ (2014) An investigation on the formation mechanism of nano ZrB_2 powder by a magnesiothermic reaction. J Alloys Compd 588:36–41. https://doi.org/10.1016/j.jallcom.2013.11.050

[46] Zhang S, Khangkhamano M, Zhang H, Yeprem HA (2014) Novel synthesis of ZrB_2 powder via molten-salt-mediated magnesiothermic reduction. J Am Ceram Soc 97:1686–1688. https://doi.org/10.1111/jace.12945

[47] Shiryaev AA (1985) Thermodynamics of SHS process: advanced approach. J Phys Chem Ref 14:1856

[48] Khanra AK (2007) Reaction chemistry during self-propagating high-temperature synthesis (SHS) of H_3BO_3–ZrO_2–Mg system. Mater Res Bull 42:2224–2229. https://doi.org/10.1016/j.materresbull.2007.01.016

[49] Zheng YT, Li HB, Xu ZH et al (2013) Reaction mechanism of self-propagating magnesiothermic reduction of ZrB_2 powders. Rare Met 32:408–413. https://doi.org/10.1007/s12598-013-0069-2

[50] Narayana Swamy AK, Shafirovich E (2014) Conversion of aluminum foil to powders that react and burn with water. Combust Flame 161:322–331. https://doi.org/10.1016/j.combustflame.2013.08.017

[51] Asamoto RR, Novak PE (1967) Tungsten-rhenium thermocouples for use at high temperatures. Rev Sci Instrum 38:1047–1052. https://doi.org/10.1063/1.1720964

[52] Grain CF (1967) Phase Relations in the ZrO_2–MgO System. J Am Ceram Soc 50:288–290. https://doi.org/10.1111/j.1151-2916.1967.tb15111.x

[53] Duwez P, Odell F, Brown Frank H (1952) Stabilization of zirconia with calcia and magnesia. J Am Ceram Soc 35:107–112

[54] Akkas B, Alkan M, Derin B, Yücel O (2011) Effect of HCl concentration on ZrB_2 separation from a self-propagating high-temperature synthesis (SHS) product. Suppl Proc 1:499–504. https://doi.org/10.1002/9781118062111.ch56

[55] Philipp WH (1966) Chemical reactions of carbides, nitrides, and borides of titanium and zirconium and chemical bonding in these compounds. NASA TN D-3533. Cleveland, OH

[56] Lee SH, Sakka Y, Kagawa Y (2008) Corrosion of ZrB_2 powder during wet processing—analysis and control. J Am Ceram Soc 91:1715–1717. https://doi.org/10.1111/j.1551-2916.2008.02343.x

[57] Khanra AK, Pathak LC, Mishra SK, Godkhindi MM (2005) Sintering of ultrafine zirconium diboride powder prepared by modified SHS technique. Adv Appl Ceram 104:282–284. https://doi.org/10.1179/174367605X52077

[58] Chamberlain AL, Fahrenholtz WG, Hilmas GE (2006) Pressureless sintering of zirconium diboride. J Am Ceram Soc 89:450–456. https://doi.org/10.1111/j.1551-2916.2005.00739.x

[59] Rahaman MN (2008) Sintering of ceramics. Taylor and Francis Group, LLC, Boca Raton

[60] Slamovich EB, Lange FF (1990) Densification behavior of single-crystal and polycrystalline spherical particles of zirconia. J Am Ceram Soc 73:3368–3375. https://doi.org/10.1111/j.1151-2916.1990.tb06463.x